Electronic Supplementary Material (ESI) for Physical Chemistry Chemical Physics.

Supporting Information for publication

Effect of cobalt phosphide (CoP) vacancies on its hydrogen evolution activity via water splitting: A theoretical study†

Xiaofei Cao[a], Yuan Tan[a], Huaan Zhen[a], Jun Hu[a*], Xi Chen[b*], Zhong Chen[c*]

[a] School of Chemical Engineering, Northwest University, Xi'an, P. R. China 710069;

[b] Earth Engineering Center, Center for Advanced Materials for Energy and Environment, Department of Earth and Environmental Engineering, Columbia University, New York NY10027, USA;

[c] School of Materials Science and Engineering, Nanyang Technological University, 50 Nanyang Avenue, Singapore 639798

Table S1. Optimized crystallographic parameters of CoP compared to experimental data. The atomic fractional coordinates of all atoms and the bond lengths are also presented.

	Crystallographic parameters				Atomic fractional coordinates		Bond length/ Å
	A(Å)	*b*(Å)	*c*(Å)	*β*(°)	Co	P	Co-P/ Å`
This work	3.242	5.032	5.480	90.00	(0.250,0.504,0.695)	(0.250,0.689,0.82)	2.315×2 2.326×2 2.327×2 2.196×2 2.247×2
Powder X-ray diffraction (295K)[S1, S2,S3]	3.281	5.077	5.587	90.00	(0.250,0.501,0.696)	(0.250,0.691,0.082)	2.348×4 2.347×2 2.206×2 2.267×2

As shown in Table S1, the simulated crystallographic parameters of the optimized orthorhombic CoP agree well with the experimental results from powder X-ray diffraction.

Table S2. Data on surface energies of different low-index surfaces. The optimization is carried out until the energy, maximum force, maximum stress, and maximum displacement are smaller than 5.0×10^{-6} eV/atom, 0.01 eV/Å, 0.02 GPa, and 5.0×10^{-4} Å, respectively. The energy cutoff is 330 eV and the SCF tolerance is 5.0×10^{-7} eV/atom.

Surface	E_{slab}(eV)	Number	Surface area(Å^2)	Surface energies (J·m^{-2})
(100)	-12241.427	$Co_{10}P_{10}$	28.177	2.497
(010)A	-14686.175	$Co_{12}P_{12}$	36.320	3.105
(010)B	-14683.680	$Co_{12}P_{12}$	36.320	3.655
(001)A	-24486.326	$Co_{20}P_{20}$	33.163	3.404
(001)B	-24486.326	$Co_{20}P_{20}$	33.163	3.404
(110)A	-17139.284	$Co_{14}P_{14}$	33.522	2.631
(110)B	-17138.771	$Co_{14}P_{14}$	33.522	2.754
(101)A	-9787.131	Co_8P_8	32.697	3.194
(101)B	-19529.001	$Co_{16}P_{16}$	32.697	2.042
(011)A	-19586.207	$Co_{16}P_{16}$	49.182	2.301
(011)B	-29384.984	$Co_{24}P_{24}$	49.182	2.528
(111)A	-14689.005	$Co_{12}P_{12}$	38.896	2.316
(111)B	-17138.449	$Co_{14}P_{14}$	38.896	2.439
(111)C	-26938.039	$Co_{22}P_{22}$	38.896	2.559

As shown in table S2, the (101)B facet has the lowest surface energy among all low-index surfaces of CoP. Usually, the lower surface energy indicates the more stable surface. The experiment also proved that the (101) surface is easily exposed facet[S4], therefore, (101)B is selected to do calculation for its high stability and easily exposed characteristics.

Table S3. Data about calculated adsorption energies of CoP (101)B surface and CoP (101)B surfaces with Co_{vac} and P_{vac}.

Adsorption	Surface	$E_{molecule+surface}$(eV)	$E_{molecule}$(eV)	$E_{surface}$(eV)	E_{ads}(eV)
	(101)B	-20061.208	-468.713	-19592.001	-0.267
H_2O*	(101)B with Co_{vac}	-19016.435	-468.713	-18546.489	-1.233
	(101)B with P_{vac}	-19879.871	-468.713	-19410.183	-0.978
	(101)B	-19608.128	-32.418	19592.001	0.081
H*	(101)B with Co_{vac}	-18562.808	-32.418	-18546.489	-0.111
	(101)B with P_{vac}	-19426.633	-32.418	-19410.183	-0.241
	(101)B	-20045.008	-449.926	19592.001	-3.071
OH*	(101)B with Co_{vac}	-19000.391	-449.926	-18546.489	-3.966
	(101)B with P_{vac}	-19863.655	-449.926	-19410.183	-3.536

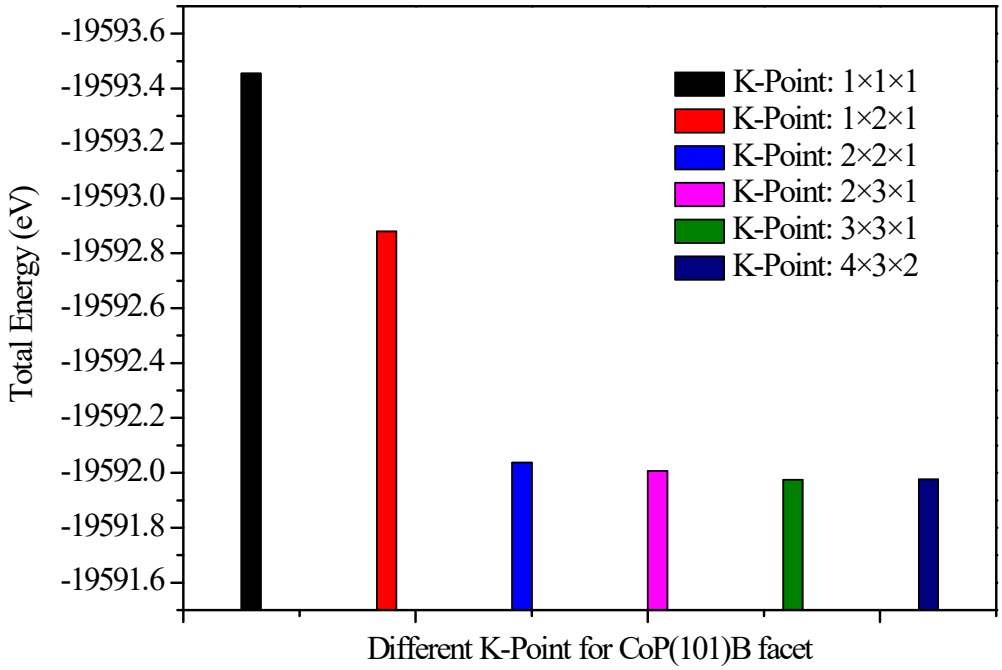

Fig. S1 The variation trend of the total energy under different K point settings.

From Fig. S1, it can be found that the total energy exists large fluctuations when the K-Point setting are rough. When the K-Point was set as 2×3×1 and more precise, the total energy no longer changes significantly. Thus, our K-Point set as 2×3×1 is reasonable.

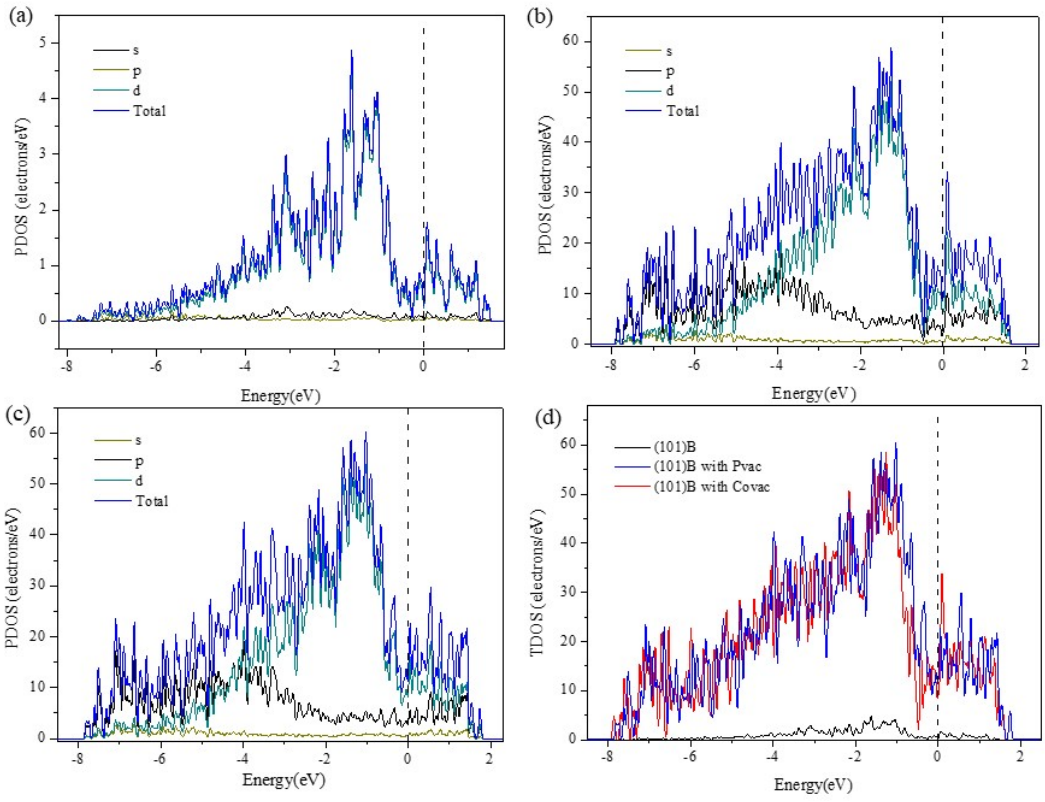

Fig. S2 (a)-(c) calculated partial density of states (DOS) for CoP(101)B, CoP(101)B with Co_{vac}

and CoP(101)B with P_{vac}. (d) the total density of states (DOS) for CoP(101)B, CoP(101)B with Co_{vac} and P_{vac}.

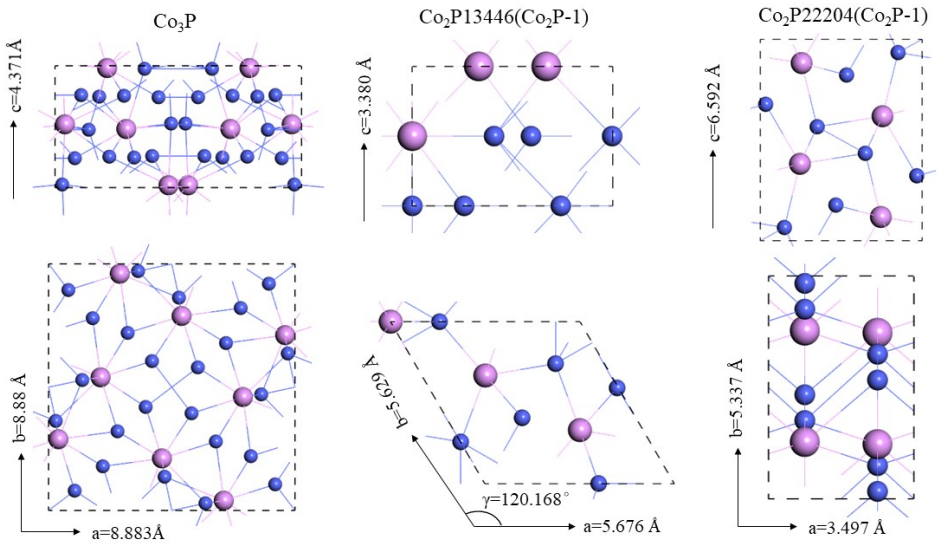

Fig. S3 The optimized crystal structure and lattice parameter of the tetragonal Co_3P, triclinic Co_2P-1 and orthorhombic Co_2P-2.

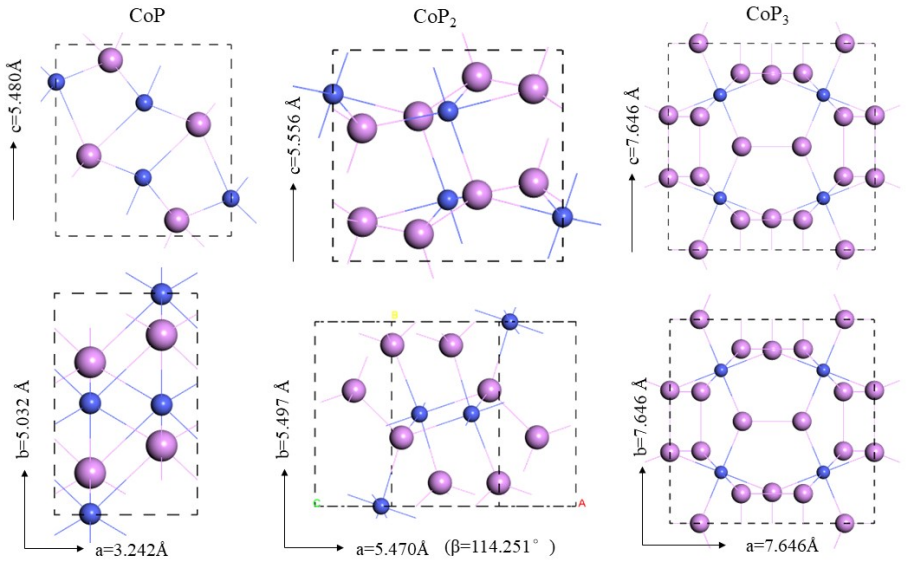

Fig. S4 The optimized crystal structure and lattice parameter of the orthorhombic CoP, triclinic CoP_2 and cubic CoP_3.

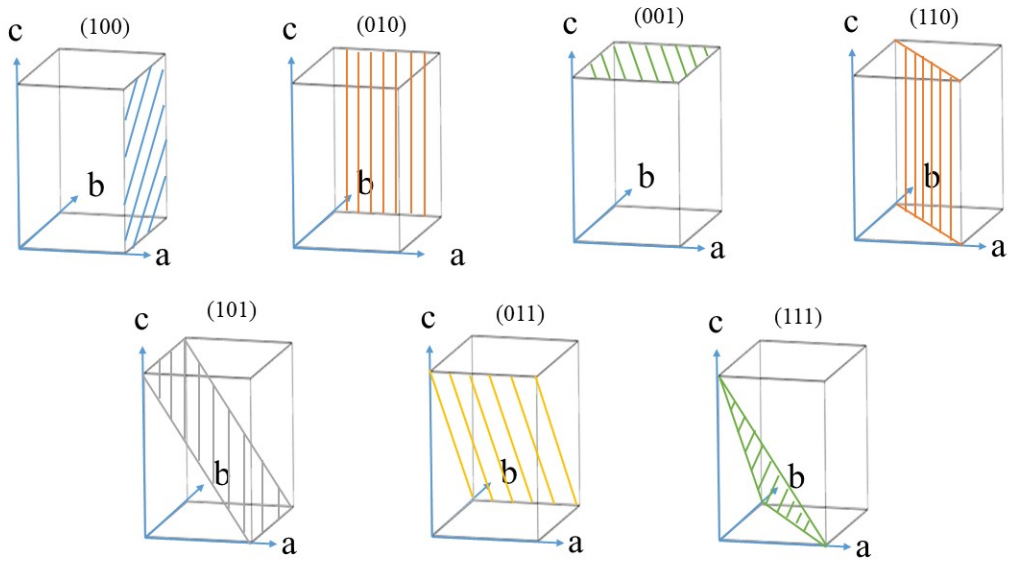

Fig. S5 The overall surfaces considered in this paper, where the equivalent surfaces are put together. Base on the symmetry of orthogonal CoP, the following planes are equivalent: (100) and (-100); (010) and (0-10); (001) and (00-1); (110), (-1-10), (-110) and (1-10); (101), (-10-1), (-101) and (10-1); (011), (0-1-1), (0-11) and (01-1); (111), (-111), (1-1-1), (11-1), (-1-11), (1-11), (-11-1) and (-1-1-1). Accordingly, we only selected the (100), (010), (001), (110), (101), (011) and (111) surface during calculation.

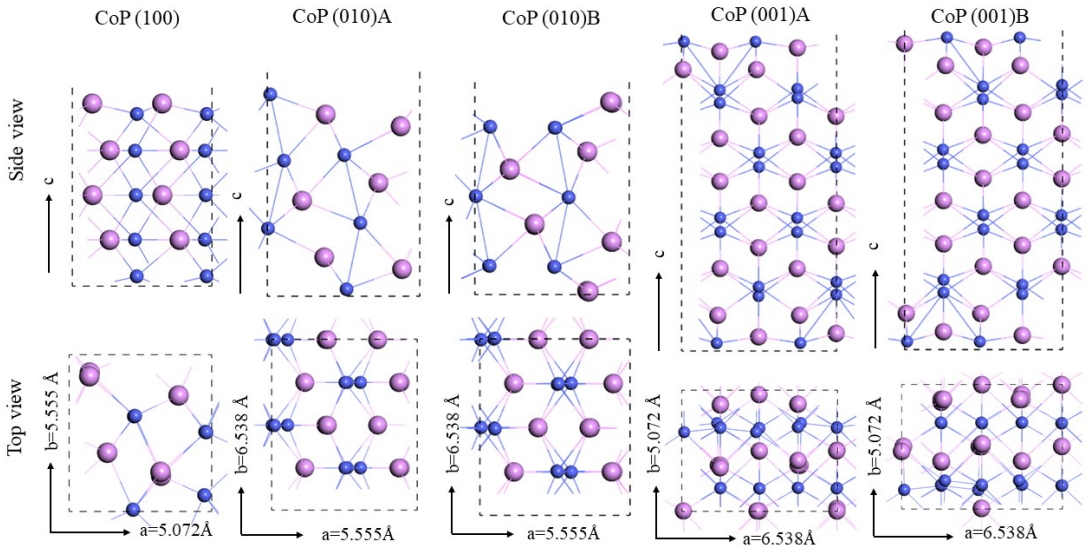

Fig. S6 Surface structure and lattice parameter of low-index (001) surface for orthogonal CoP. Bi (purple) and O (bule) atoms are shown in colored spheres.

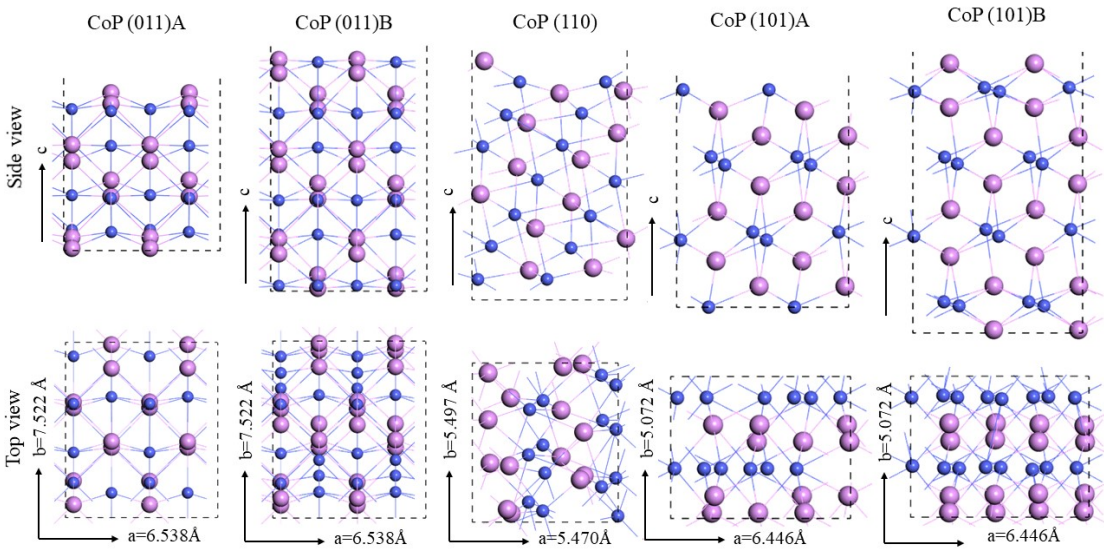

Fig. S7 Surface structure and lattice parameter of low-index surface (101) for orthogonal CoP. Bi (purple) and O (bule) atoms are shown in colored spheres.

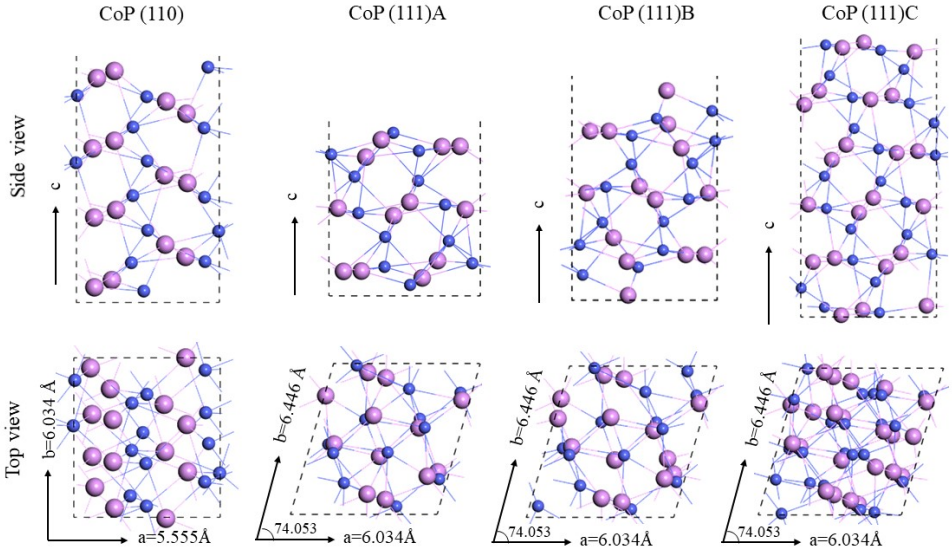

Fig. S8 Surface structure and lattice parameter of low-index surface for orthogonal CoP. Bi (purple) and O (bule) atoms are shown in colored spheres.

All low-index surfaces of orthogonal CoP are showed in Figure S6-S7, each low-index surface may contain several kinds of terminations, all facets are stoichiometric surfaces.

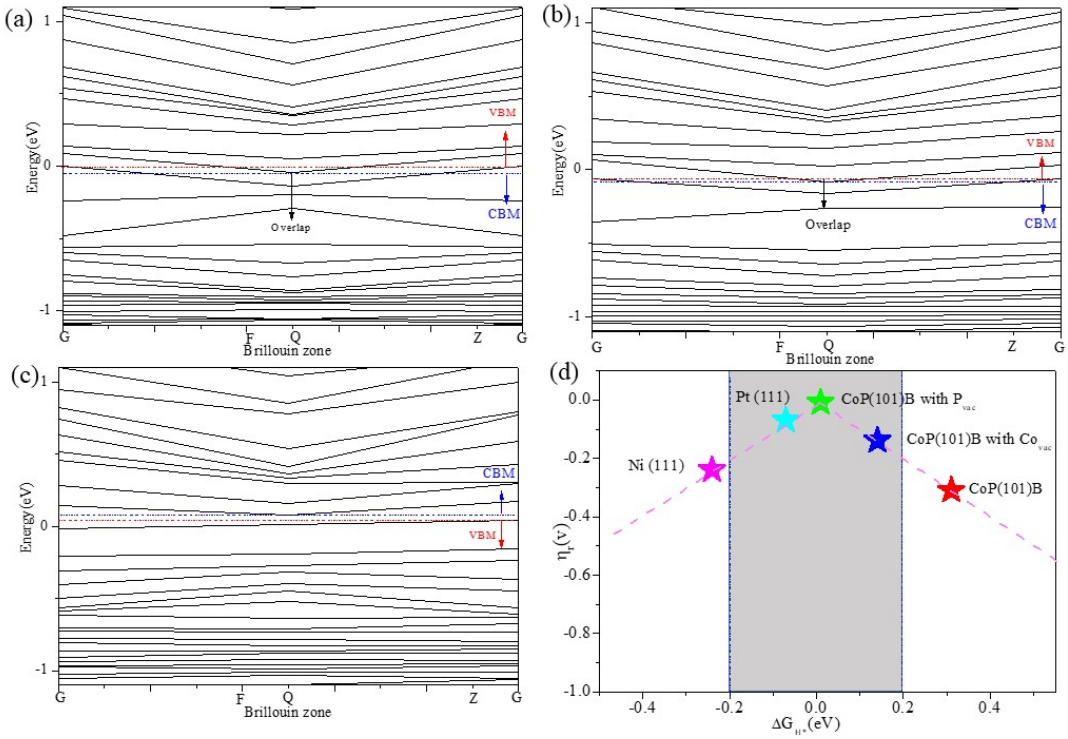

Fig. S9 (a) Calculated band structure of CoP (101)B surface, (b) band structure of CoP (101)B surface with Co_{vac}, (c) band structure of CoP (101)B surface with P_{vac}. (d) Calculated HER volcano plot for perfect CoP (101)B surface, CoP (101)B surface with Co_{vac} and P_{vac}. The overpotential of CoP(101)B facet with P_{vac} is lower that Pt (111), it is an ideal catalyst for hydrogen production form electrocatalytic water splitting.

S1 T. Liu, P, Li, N, Yao, et al. *Angewandte Chemie-international Edition*, 2019, **14**，131.
S2 X. Huang, X. Xu, X. Luan, et al. *Nano Energy*, 2019, **68**, 104332.
S3 C. Tang, Z. Rong, W. Lu, et al. *Advanced Materials*, 2016, **2**, 29.
S4 X. Huang, X. Xu, X. Luan, et al. *Nano Energy*, 2019, **68**, 104332.